Dalton Transactions

ROYAL SOCIETY OF CHEMISTRY

PAPER

View Article Online
View Journal | View Issue

Cite this: *Dalton Trans.*, 2022, **51**, 9994

Synthesis, solid-state, solution, and theoretical characterization of an "in-cage" scandium-NOTA complex†

Kelly E. Aldrich,[a] Ivan A. Popov,[a,b] Harrison D. Root,[a] Enrique R. Batista,*[a] Samuel M. Greer,[a] Stosh A. Kozimor,*[a] Laura M. Lilley,[a] Maksim Y. Livshits,[a] Veronika Mocko,[a] Michael T. Janicke,[a] Brian L. Scott,[a] Benjamin W. Stein[a] and Ping Yang*[a]

Developing chelators that strongly and selectively bind rare-earth elements (Sc, Y, La, and lanthanides) represents a longstanding fundamental challenge in inorganic chemistry. Solving these challenges is becoming more important because of increasing use of rare-earth elements in numerous technologies, ranging from paramagnets to luminescent materials. Within this context, we interrogated the complexation chemistry of the scandium(III) (Sc^{3+}) trication with the hexadentate 1,4,7-triazacyclononane-1,4,7-triacetic acid (H_3NOTA) chelator. This H_3NOTA chelator is often regarded as an underperformer for complexing Sc^{3+}. A common assumption is that metalation does not fully encapsulate Sc^{3+} within the $NOTA^{3-}$ macrocycle, leaving Sc^{3+} on the periphery of the chelate and susceptible to demetalation. Herein, we developed a synthetic approach that contradicted those assumptions. We confirmed that our procedure forced Sc^{3+} into the $NOTA^{3-}$ binding pocket by using single crystal X-ray diffraction to determine the Na[Sc(NOTA)($OOCCH_3$)] structure. Density functional theory (DFT) and ^{45}Sc nuclear magnetic resonance (NMR) spectroscopy showed Sc^{3+} encapsulation was retained when the crystals were dissolved. Solution-phase and DFT studies revealed that $[Sc(NOTA)(OOCCH_3)]^{1-}$ could accommodate an additional H_2O capping ligand. Thermodynamic properties associated with the Sc-$OOCCH_3$ and Sc-H_2O capping ligand interactions demonstrated that these capping ligands occupied critical roles in stabilizing the [Sc(NOTA)] chelation complex.

Received 16th November 2021,
Accepted 19th May 2022

DOI: 10.1039/d1dt03887g

rsc.li/dalton

Introduction

Recent advances in inorganic chemistry have supported development of a wide range of technologies based on rare-earth elements (Sc, Y, La, and lanthanides).[1–6] This application space spans from superconducting materials and paramagnets[7–9] to luminescent technologies[10–12] as well as radiotherapeutics and radiodiagnostics.[13–24] To advance the state-of-the-art in the aforementioned rare earth technologies, there is need to develop a better understanding of rare-earth element chemistry, in general. One area in need of attention is associated with rare-earth chelation. On the fundamental side, identifying chelators that bind strong and selective to Sc^{3+}, Y^{3+}, Lu^{3+}, and the rest of the 4f-elements represents a longstanding challenge in inorganic chemistry. On the applied front, rare-earth chelation chemistry is important for purifying rare-earth elements in large-scale processing, remediating environmental contamination areas, and quantitatively analyzing for rare-earth elements in analytical samples.

Breakthroughs in the radiopharmaceutical field have ignited recent interest in complexing one particular rare-earth element, namely Sc^{3+}. The ^{44}Sc and ^{43}Sc isotopes are promising agents for positron emission tomography (PET) imaging and ^{47}Sc is a potential therapeutic that emits low energy Auger electrons.[13,25–33] Pharmaceutically relevant scandium chelators need to bind Sc^{3+} rapidly, irreversibly, under mild conditions, and in high yield.[34] Most Sc^{3+} chelator design and metalation strategies are based on successful lanthanide chelation chemistry because Sc^{3+} shares many physical properties with lanthanide(III) cations. These characteristics include a highly stable

[a]*Los Alamos National Laboratory, Los Alamos, NM, USA. E-mail: erb@lanl.gov, stosh@lanl.gov, pyang@lanl.gov*
[b]*Department of Chemistry, The University of Akron, Akron, Ohio 44325-3601, USA*

†Electronic supplementary information (ESI) available: NMR spectra including fits for VT NMR; additional discussion of X-Ray diffraction data; additional information on the computed reactions and method details. CIF files for *SOLUTION_1* of the solid-state single crystal structure. CCDC 2072300 and 2076191. For ESI and crystallographic data in CIF or other electronic format see DOI: https://doi.org/10.1039/d1dt03887g

+3 oxidation state, oxophilicity, and strong Lewis acidity. From this perspective, it is not surprising that many previous studies repurposed common lanthanide chelators for application with Sc^{3+}. Some representative examples are provided in Chart 1; *e.g.* diethylenetriaminepentaacetic acid, H_5DTPA, 1,4,7,10-tetraazacyclododecane-1,4,7,10-tetraacetic acid, H_4DOTA, and AAZTA.[35–38]

Despite strong similarities between Sc^{3+} and the other rare-earth elements, scandium is a first-row transition metal, which leads to significant differences compared to the lanthanides. It has valence 3d-orbitals, not 4f- and 5d-orbitals. It is also much smaller than the 4f-elements and, consequently, more Lewis acidic. For example, the eight-coordinate ionic radius for Sc^{3+} (0.87 Å) is over 0.3 Å smaller than the largest lanthanide (La^{3+} at 1.18 Å) and 0.1 Å smaller than the smallest lanthanide (Lu^{3+} at 0.97 Å).[39] We propose that these distinctions should endow Sc^{3+} with chemical characteristics that can be tailored specifically to Sc^{3+} chelation and worry that treating Sc^{3+} as a small lanthanide is an oversimplification that limits innovation in Sc^{3+} chelator design. Within this context, we questioned why the small, hexadentate chelate H_3NOTA (1,4,7-triazacyclononane-1,4,7-triacetic acid) was not more routinely used in Sc^{3+} chemistry. Reviewing the literature suggested $NOTA^{3-}$ often underperforms in Sc^{3+} binding, especially when compared to the larger $DOTA^{4-}$ chelate.[35–38] This underperformance has been attributed to $NOTA^{3-}$ binding Sc^{3+} in a labile fashion, which is correlated with $NOTA^{3-}$ failing to encapsulated Sc^{3+} into its binding pocket where Sc^{3+} can interact with both the pendent acetate functional groups and the triaza-macrocyclic backbone (Chart 1). In the alternative and undesirable "out-of-cage" binding, Sc^{3+} only interacts with the acetate functional groups.[36,38,40,41] Only by modifying NOTA's acetate substituents (*e.g.* longer linkers or alternate metal binding functionality) has "in-cage", stable and robust Sc^{3+} binding been consistently realized with the 1,4,7-triaazacylcononane backbone of NOTA.[34,42–44]

Herein, we undertook a coordination chemistry study focused on better understanding Sc^{3+} complexation chemistry with $NOTA^{3-}$. We synthesized an "in-cage" complex and used numerous characterization techniques to probe the interactions between Sc^{3+} and $NOTA^{3-}$. For example, the solid-state structure of $[Sc(NOTA)(OOCCH_3)]^{1-}$ was determined, for the first time, using single crystal X-ray diffraction. Subsequently, we showed that "in-cage" Sc^{3+} binding by $NOTA^{3-}$ was pre-

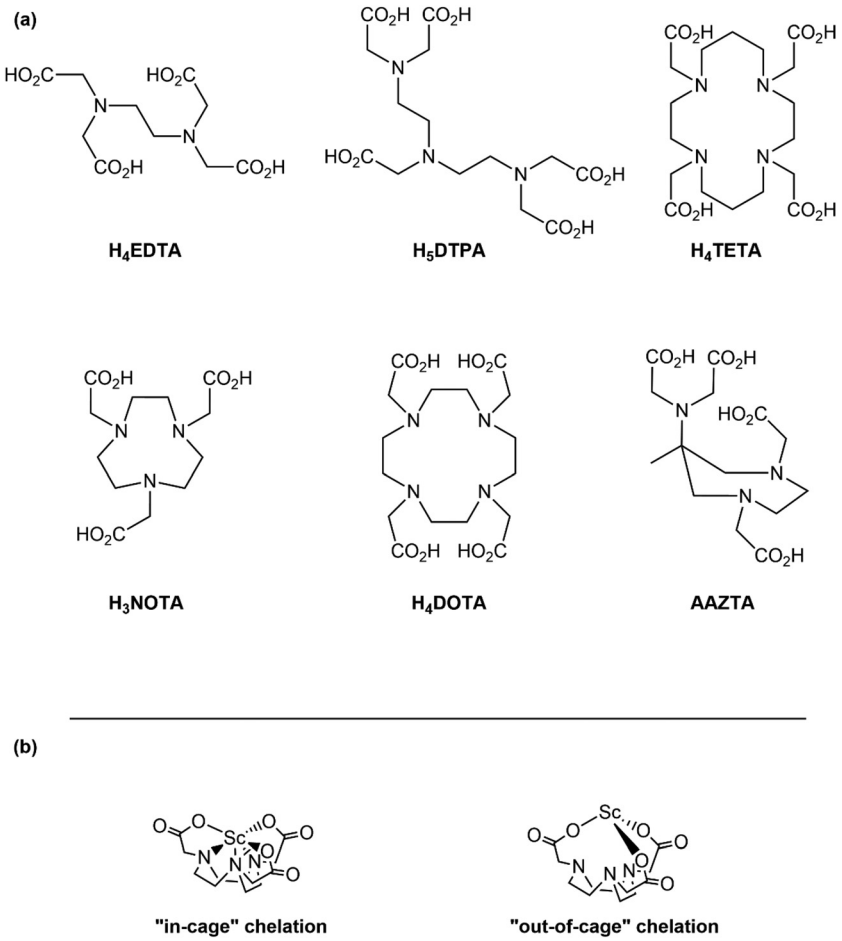

Chart 1 (a) Examples of some common chelates previously considered as Sc^{3+} binding agents; (b) an illustration of Sc^{3+} bound "in-cage", with full chelation by the macrocycle, *vs.* "out-of-cage" with interactions between only the metal and pendant acetate arms.

served in aqueous solution, using ^{45}Sc NMR spectroscopy. Interpretation of the solution phase data was guided by theoretical studies that, when combined with experimental results, provided insight into the behavior of the [Sc(NOTA)] complex in aqueous solutions. These studies also highlighted the critical role of capping ligand(s), defined here as ligands occupying vacant coordination sites after metalating a chelator. For example, we observed that the capping acetate and H_2O ligands were more than arbitrary ancillary binding agents that filled out Sc^{3+}'s first coordination sphere. Instead, coordination of the capping ligands, specifically acetate, contributed substantially to the overall stability of the "in-cage" [Sc(NOTA)] chelation complex.

Results and discussion

Synthesis of Na[Sc(NOTA)(OOCCH$_3$)]

Sodium scandium(III) 1,4,7-triazanonane-1,4,7-triacetate κ^2-acetate, Na[Sc(NOTA)(OOCCH$_3$)], was prepared from a reaction that fully encapsulated Sc^{3+} into 1,4,7-triazacyclononane-1,4,7-triacetate ($NOTA^{3-}$). The resulting complex contained both Sc–O_{NOTA} and Sc–N_{NOTA} bonds (Scheme 1). Our experimental procedure was carried out under mild conditions. Metalation was achieved in aqueous media, under ambient atmosphere (air), using low temperatures, and in an aqueous solution that had been adjusted to a slightly acidic pH [acetate buffer, $HOOCCH_3$/$NaOOCCH_{3(aq)}$; 0.1 M; pH of 5]. Under these conditions H_3NOTA·3 HCl (1 equivalent) was combined with anhydrous scandium(III) triflate, $Sc(OTf)_3$ (1 equivalent), and heated mildly (at 50 °C) for several hours to drive the reaction as far as possible toward complete complexation of Sc^{3+} by $NOTA^{3-}$. This approach achieved high-yielding (~70% isolated) and complete Sc^{3+} complexation with a 1 : 1 ligand to metal ratio.

After heating, a small amount of free $Sc^{3+}_{(aq)}$ (not complexed) was easily removed from the reaction mixture. This was achieved by precipitation of the uncomplexed Sc^{3+}, which occurred rapidly when the pH was raised to 8 by addition of aqueous sodium hydroxide [$NaOH_{(aq)}$, 1 M, K_{sp} for $Sc(OH)_3$ = 2.22×10^{-31}].[39] The resultant fine, white precipitate was removed *via* filtration and the filtrate was collected. Subsequent removal of the volatiles *in vacuo* left a white residue that contained a mixture of leftover reagents ($NaOOCCH_3$, NaOH), byproducts (NaOTf and NaCl), and the Na[Sc(NOTA)(OOCCH$_3$)] target compound. Purification of the Sc^{3+} complex from these salts required extraction of the reaction residue with a solvent mixture of methanol and water (1 : 1) followed by crystallization at reduced temperature (10 °C, 1 week), with acetone added as an antisolvent. This crystallization method yielded plate-like, colorless single crystals.

Solid-state characterization with single crystal X-Ray diffraction

Analysis of the colorless plates by single crystal X-ray diffraction confirmed formation of Na[Sc(NOTA)(OOCCH$_3$)]. The crystallographic data were modeled in a C-centered, monoclinic crystal system in the *C*2/*c* space group. This model showed two

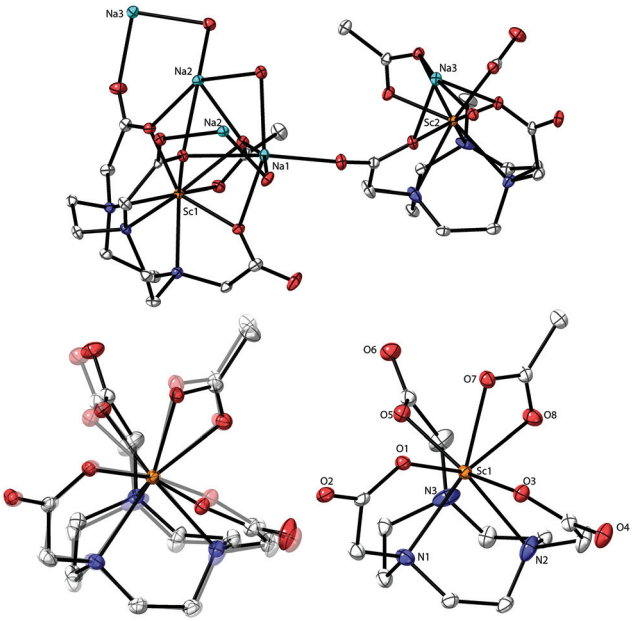

Fig. 1 Single crystal X-ray structure of Na[Sc(NOTA)(OOCCH$_3$)]; Sc = orange, Na = aquamarine, N = blue, O = red, C = grey. Thermal ellipsoids are shown at 50% probability. Calculated H-atoms and disordered $-CH_2-$ groups on the $NOTA^{3-}$ backbone were omitted for clarity. Top – Asymmetric unit contents are shown, with two full $[Sc(NOTA)(OOCCH_3)]^{1-}$ units bridged by Na^{1+} cations *via* carbonyl oxygens of the $NOTA^{3-}$ ligand and $OOCCH_3^{1-}$. Bottom left – An overlay showing that the geometries for Sc1 are similar to Sc2 within the $[Sc(NOTA)(OOCCH_3)]^{1-}$ substructure. Bottom right – The geometry of Sc1 in $[Sc(NOTA)(OOCCH_3)]^{1-}$. Data is from solution 1.

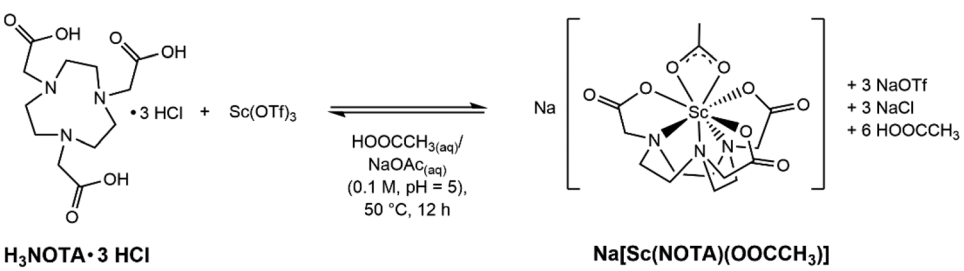

Scheme 1 Synthesis of Na[Sc(NOTA)(OOCCH$_3$)] complex in acetate buffered solution.

$[Sc(NOTA)(OOCCH_3)]^{1-}$ anions within the asymmetric unit (Fig. 1) that had nearly identical structures (see ESI† for more discussion on this topic). They each contained a single Sc^{3+} cation bound by the hexadentate $NOTA^{3-}$ chelate. There were three Sc–N_{NOTA} bonds associated with the cyclic aza-macrocycle and three Sc–O_{NOTA} bonds from the acetate arms. Although this binding motif is prototypical of complete metal binding by polyaza acetate chelators,[38,42,45–47] it has not been previously observed for $NOTA^{3-}$ binding of Sc^{3+}. The three acetate arms and their corresponding nitrogen atoms (from the macrocycle) were eclipsed, rather than twisted.[48–51] Each [Sc(NOTA)] fragment was additionally capped by an acetate ligand (κ^2-$OOCCH_3{}^{1-}$) bound through both acetate oxygen atoms. This ligand environment around Sc^{3+} provided a total coordination number of eight, a common aqueous coordination number for Sc^{3+}. Constraints imposed by the alkyl linkages of the hexadentate chelator ($NOTA^{3-}$) and the capping ligand (κ^2-$OOCCH_3{}^{1-}$) prevented adaptation of an idealized 8-coordinate geometry for Sc^{3+} bound O and N atoms. Instead, the Sc^{3+} inner coordination sphere contained five O and three N atoms arranged somewhere between a bicapped trigonal antiprism (C_{2v}) and a dodecahedron (D_{2d}). These restrictions imparted low molecular symmetry. We identified only one pseudo-reflection plane, which contained the Sc^{3+} cation and the planar κ^2-$OOCCH_3{}^{1-}$ ligand, and no rotational axes within each anionic fragment. Based on these findings, it seemed most appropriate to describe the $[Sc(NOTA)(OOCCH_3)]^{1-}$ anion fragment using the C_s point group.

Looking beyond the first few coordination spheres revealed that the $[Sc(NOTA)(OOCCH_3)]^{1-}$ anions were arranged in two-dimensional sheets that extend parallel to the *bc*-plane (Fig. 2). Within each sheet, $[Sc(NOTA)(OOCCH_3)]^{1-}$ anions were linked through a multifaceted Sc–O···Na···O=C–O–Sc network that sandwiched the Na^{1+} cations between $[Sc(NOTA)(OOCCH_3)]^{1-}$ anions. This arrangement caused the boundary of each sheet along the *bc*-plane to consist of hydrophobic CH_2 groups from the macrocyclic NOTA-backbone (polyaza ring). Within the sandwich, the Na^{1+} cations were bridged by $NOTA^{3-}$ oxygen atoms that were not directly bound to Sc^{3+} (terminal carbonyl-like oxygens), as well as linkages involving both of the acetate oxygen atoms bound to Sc^{3+} in each anion fragment. Although the sum-total Na^{1+} coordination number (for each Na^{1+} atom) was six, the geometries around each Na^{1+} cation were not regular nor did they fall into idealized six-coordinate geometries (*i.e.* not perfectly octahedral or trigonal anitprismatic).

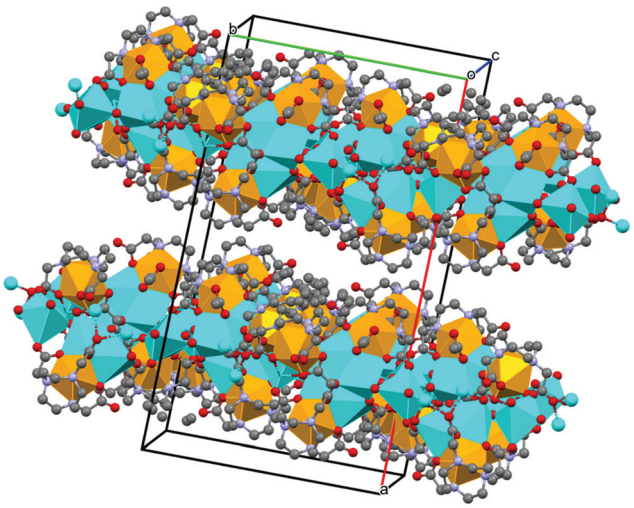

Fig. 2 Extended structure of $Na[Sc(NOTA)(OOCCH_3)]$ with sheets of $[Sc(NOTA)(OOCCH_3)]_x^{1-}$ linked through Na^{1+} cations; Sc = orange, Na = aqua, N = blue, O = red, C = grey. The unit cell is shown and first-coordination sphere for Sc^{3+} and Na^{1+} have been represented as orange and aqua polyhedra, respectively. Calculated H-atoms were omitted for clarity.

Many molecules of water (H_2O) filled the void spaces between consecutive $Na[Sc(NOTA)(OOCCH_3)]$ layers. Exact numbers and positions of H_2O molecules were difficult to determine. Hence, we investigated two crystallographic solutions. In the first model, solution 1, the electron density within the void space was treated using the "squeeze" function in Olex2 refinement software (with Platon, running ShelX refinement package).[52–54] In the second model, solution 2, the residual void space electron density was modeled with discrete H_2O molecules. Interatomic distances and angles for $Na[Sc(NOTA)(OOCCH_3)]$ from the two different models were essentially indistinguishable and largely fell within the uncertainty of the solution statistics. Solution 1 gave a slightly lower *R*-value compared to solution 2, R_1 = 0.0427 *vs.* 0.0608. Based on this metric, we only included bond distances and angles from solution 1 herein. Related to this topic is a subtle detail associated with the $Na[Sc(NOTA)(OOCCH_3)]$ structure. Three Na^{1+} cations co-crystalized alongside two $Sc(NOTA)(OOCCH_3)^{1-}$ anions. The system charge balances with one of the interstitial "water" molecules likely being a hydroxide (OH^{1-}). Given the quality of the data, no attempt was made to model the position of the OH^{1-} or the accompanying and likely proton disorder.

Investigation of solution structure with ^{45}Sc NMR

A series of scandium-45 (^{45}Sc) nuclear magnetic resonance (NMR) measurements were made to determine if the solid-state $[Sc(NOTA)(OOCCH_3)]^{1-}$ structure described above persisted in solution. These studies exploited the unique accessibility of ^{45}Sc NMR spectroscopy. First, the nuclear properties of naturally occurring ^{45}Sc made it well suited for NMR spectroscopy: 100% abundant, nuclear spin of 7/2, quadrupole moment of $-0.22b$, and a magnetogyric ratio ($\gamma_{45\text{-}Sc}$) of 6.5081 × 10^7 rad T^{-1} s^{-1} ($0.3\gamma_{1\text{-}H} = \gamma_{45\text{-}Sc}$).[55,56] Second, the ^{45}Sc NMR experiment could be conducted with common instrumentation because the ^{45}Sc NMR excitation frequency is very close to that of the more commonly probed ^{13}C nuclide (24.97% *vs.* 25.14% frequency ratios, respectively). This property makes standard broadband probes that have low frequency channels for ^{13}C data acquisition compatible with ^{45}Sc NMR experiments.

The ^{45}Sc NMR spectrum from single crystals of $Na[Sc(NOTA)(OOCCH_3)]$ dissolved in deuterated water (D_2O) showed an intense resonance at 88.8 ppm (top, Fig. 3). This

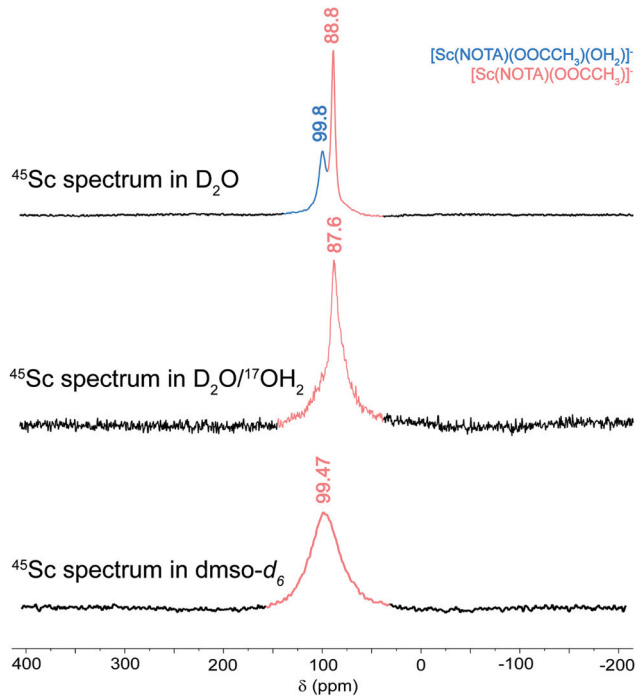

Fig. 3 ^{45}Sc NMR spectra from single crystals of Na[Sc(NOTA)(OOCCH$_3$)] dissolved in D_2O (top), D_2O with $H_2{}^{17}O$ (middle), and DMSO-d_6 (bottom). Spectra were collected at 20 °C with an operating frequency of 97 MHz. For additional discussion of the DMSO-d_6 spectrum, see ESI.†

chemical shift was comparable to those reported previously from other examples of Sc^{3+} cations completely encapsulated by related chelating agents, *e.g.* Sc(DOTA) at 90 ppm, Sc(DTPA) at 79 ppm, Sc(DO3AP) at 100 ppm, and Sc(AAZTA) at 80 ppm.[38,41,42] This good agreement suggested that upon dissolution, the Sc^{3+} cation remained encapsulated by the $NOTA^{3-}$ chelate, like the "in-cage" solid-state structure described above and depicted in Scheme 1. Consistent with this observation was the mismatch between our ^{45}Sc chemical shifts and those reported for the "out-of-cage" complexation of Sc^{3+} by polyaza acetic acid ligands. Of specific relevance were the observations made by Huclier-Markai and co-workers.[36] Those researchers observed [Sc(NOTA)] as an intermediate to "out-of-cage" complex, which had a diagnostic resonance shifted far up-field, near 20 ppm. That shift was similar, within 10 ppm, to Sc(oxalate)$_4{}^{5-}$ and the related "out-of-cage" Sc(DO3AP).[38,41] Hence, the complexation method used by Huclier-Markai and co-workers led to "out-of-cage" Sc^{3+} binding, while the method used in the present work leads to "in-cage" Sc^{3+} binding.

We attributed the resonance at 88.8 ppm to the $[Sc(NOTA)(OOCCH_3)]^{1-}$ compound. However, the small downfield shoulder at 99.8 ppm clearly indicated that there was an additional ^{45}Sc complex present in solution, one also encapsulated "in-cage" by the $NOTA^{3-}$ chelate (as indicated by the chemical shift). These signals were successfully deconvoluted using Gaussian fitting (in MestreNova V.14.1), which showed the 88.8 to 99.8 ppm peak intensity ratio was about 1.5 to 1 at 20 °C. The ^{45}Sc spectrum also showed dependence on temperature (see Fig. S5–7† and discussion below). Increasing the temperature from 20 to 80 °C shifted the peak positions determined by Gaussian deconvolution slightly (Δ < 1 ppm). More significantly, increasing temperature also caused the peak at 99.8 ppm to decrease in intensity relative to the peak at 88.8 ppm. This behavior suggested the Sc^{3+} species associated with these two features were related by a dynamic exchange process in solution. We speculated that this exchange subtly altered the first coordination sphere of $[Sc(NOTA)(OOCCH_3)]^{1-}$ (responsible for the peak at 88.8 ppm). Given that both resonances were consistent with Sc^{3+} encapsulation by $NOTA^{3-}$, this first coordination sphere change was reasonably associated with the capping ligand. Likely processes responsible for the two peaks were (1) slipping the acetate from bidentate κ^2-$OOCCH_3{}^{1-}$ to monodentate κ^1-$OOCCH_3{}^{1-}$, (2) hydration to add Sc-(H_2O) bonding interactions (Fig. 4a), or (3) substitution of the capping acetate ligand with water (Fig. 4b). The following experiments and computational studies (*vide infra*) suggested that contributions from scenarios 1 and 2 were most likely responsible for the observed exchange behavior (Fig. 4a), while scenario 3 was significantly unfavorable (Fig. 4b).

To more precisely characterize the origin of the two ^{45}Sc resonances, two additional experiments were carried out. First, the NMR solvent was changed from D_2O to DMSO-d_6. The ^{45}Sc NMR spectrum obtained from single crystals of Na[Sc(NOTA)(OOCCH$_3$)] dissolved in DMSO-d_6 showed a single broad feature at 99.47 ppm. We attributed this feature to the anhydrous $[Sc(NOTA)(OOCCH_3)]^{1-}$ complex (see ESI†). This observation reinforced our conclusion that dissolving the crystalline material generated a solution that contained a single ^{45}Sc species of the general formal $[Sc(NOTA)(OOCCH_3)]^{1-}$; however, we acknowledged that a DMSO adduct was also possible. The second ^{45}Sc NMR experiment resembled the original measurement shown in Fig. 3 in that Na[Sc(NOTA)(OOCCH$_3$)] crystals were dissolved in D_2O. However, this solution was spiked with ^{17}O isotopically enriched $H_2{}^{17}O$ (10 μL at 90% enrichment). The quadrupolar ^{17}O nucleus (spin 5/2) provided an opportunity to identify if Sc-(H_2O) bonds formed in solution. Close contact between the quadrupolar ^{17}O and ^{45}Sc nuclei through Sc-(H_2O) interactions should enhance spin–spin relaxation, shorten the nuclear relaxation times (T_2) for interacting ^{17}O and ^{45}Sc nuclei during the NMR experiment, and dramatically broaden the observed ^{45}Sc NMR resonance.[55,56] As demonstrated in Fig. 3, this prediction aligned well with the changes observed spectroscopically upon inclusion of $H_2{}^{17}O$. The ^{45}Sc NMR spectrum in D_2O spiked with $H_2{}^{17}O$ showed a single resonance at 87.6 ppm. Meanwhile, the downfield shoulder at 99.8 ppm vanished into the baseline, likely owing to formation of Sc–$^{17}O_{H2O}$ bonds. Reasonable attempts to deconvolute the spectrum with two Gaussians failed, indicating that the remaining signal intensity at 87.6 ppm originated from a single ^{45}Sc species.

Based on the above experimental results (and the calculations described below), we concluded that the ^{45}Sc NMR

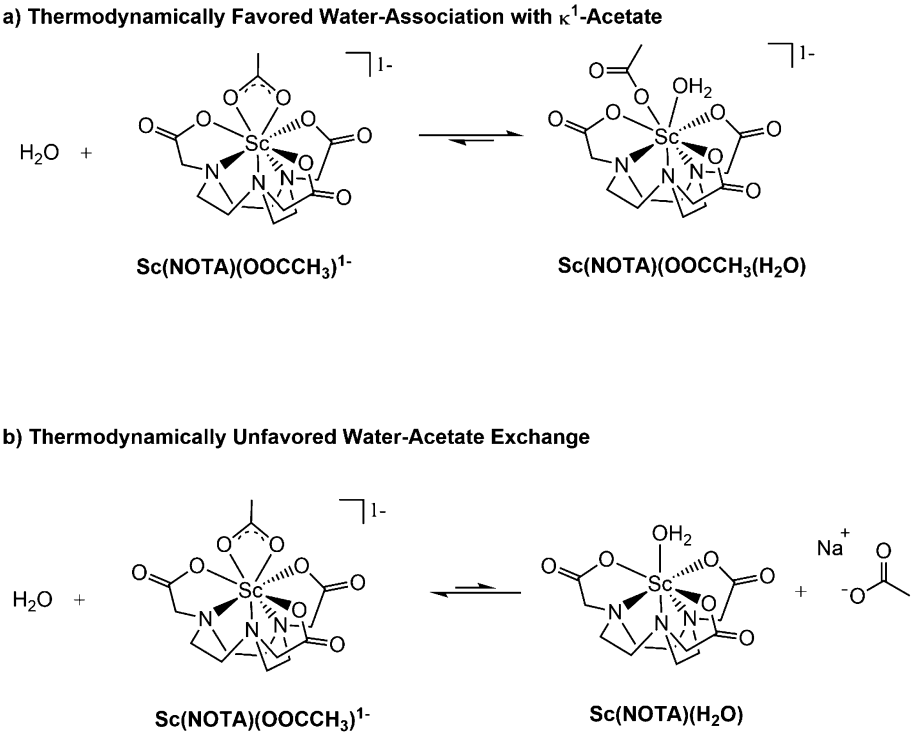

Fig. 4 Two possible interpretations of the equilibrium process observed by ^{45}Sc NMR spectroscopy of Na[Sc(NOTA)(OOCCH$_3$)] crystals dissolved in D_2O. The aqueous environment gives rise to two species of varying concentrations in solution; (a) coordination of water without loss of the acetate ligand *vs.* (b) exchange of the capping acetate ligand for water. Note, our analyses suggest that process (a) is the primary exchange process accessible in aqueous solutions.

spectrum showed a combination of two species that coexisted in H_2O solutions on the ^{45}Sc NMR time scale. Two possible scenarios for this exchange process were presented in Fig. 4. The major contributor to the spectrum at room temperature was the anhydrous $[Sc(NOTA)(OOCCH_3)]^{1-}$ that exhibited the ^{45}Sc resonance near 88 ppm. There was also a minor species that exhibited a ^{45}Sc resonance near 100 ppm, namely the hydrated $[Sc(NOTA)(OOCCH_3)(H_2O)]^{1-}$ (Fig. 4a). The data showed the Sc^{3+} cation in both $[Sc(NOTA)(OOCCH_3)(H_2O)]^{1-}$ and $[Sc(NOTA)(OOCCH_3)]^{1-}$ resided in the binding pocket of $NOTA^{3-}$, akin to the solid-state structure (*vide supra*), as evident from the dramatic downfield shifts of both species relative to the $Sc(NO_3)_3(H_2O)_x$ standard (0 ppm). The only observable difference between the two coordination complexes was the presence of an H_2O ligand in $[Sc(NOTA)(OOCCH_3)(H_2O)]^{1-}$ (Fig. 4a). The experimental data did not provide insight into the Sc-$OOCCH_3$ binding mode and ^{1}H and ^{13}C NMR spectra did not generate additional insight. Hence, we have refrained from speculating on the degree of mono- *vs.* bidentate character associated with the Sc-$OOCCH_3$ interaction (in either species) and simply acknowledge that both are possible in solution.

Experimental approximation of H_2O coordination thermodynamics

Characterizing the solution-phase exchange process between $[Sc(NOTA)(OOCCH_3)]^{1-}$ (88.8 ppm, linewidth = 450 Hz) and $[Sc(NOTA)(OOCCH_3)(H_2O)]^{1-}$ (99.8 ppm, linewidth = 880 Hz) by variable temperature ^{45}Sc NMR spectroscopy (in D_2O) provided an estimate of the thermodynamic properties associated with the H_2O coordination process (note, chemical shifts dependence on temperature were reversible). This was achieved after assuming that these two ^{45}Sc species had similar quadrupolar relaxations, which seemed reasonable owing to similar chemical shifts, linewidths, and coordination environments. Hence, a Van't Hoff approximation for the thermodynamic parameters associated with the H_2O coordination process (Fig. 4a) was generated from the following equations:

$$\ln(K_{eq}) = \frac{-\Delta H}{R} \cdot \left(\frac{1}{T}\right) + \frac{\Delta S}{R} \quad (1)$$

$$K_{eq} = \frac{a_{Sc(NOTA)(OOCCH_3)(H_2O)^{1-}}}{[a_{Sc(NOTA)(OOCCH_3)^{1-}}][a_{H_2O}]} \approx \frac{Sc(NOTA)(OOCCH_3)(H_2O)^{1-}}{Sc(NOTA)(OOCCH_3)^{1-}} \quad (2)$$

Here, K_{eq} was the equilibrium constant, R was the ideal gas constant (1.987×10^{-3} kcal mol^{-1} K^{-1}), T was temperature (Kelvin), and ΔH and ΔS were the enthalpy and entropy changes for the exchange process, respectively. Plotting the dependence of K_{eq} on $\frac{1}{T}$ showed a linear relationship over the temperature region probed (Fig. 5). A linear fit of the data gave a $\Delta H = -1.7 \pm 0.2$ kcal mol^{-1} as described in eqn (1) and ΔS =

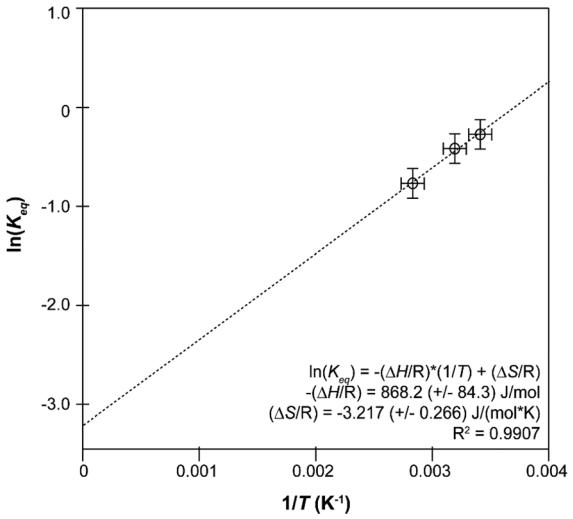

Temp (°C)	Species	Chemical Shift (ppm)	Area %
20	$[Sc(NOTA)(OOCCH_3)(H_2O)]^{1-}$	99.9	43.2
	$[Sc(NOTA)(OOCCH_3)]^{1-}$	88.6	56.8
40	$[Sc(NOTA)(OOCCH_3)(H_2O)]^{1-}$	99.9	39.7
	$[Sc(NOTA)(OOCCH_3)]^{1-}$	89.1	60.3
80	$[Sc(NOTA)(OOCCH_3)(H_2O)]^{1-}$	101.8	31.7
	$[Sc(NOTA)(OOCCH_3)]^{1-}$	90.0	68.3

Fig. 5 Top: A Van't Hoff analysis of the equilibrium constant (K_{eq}) that relates conversion of $[Sc(NOTA)(OOCCH_3)]^{1-}$ to $[Sc(NOTA)(OOCCH_3)(H_2O)]^{1-}$. Metrics from this plot were used to solve eqn (1) and (2). Bottom: Normalized distribution of the minor $[Sc(NOTA)(OOCCH_3)(H_2O)]^{1-}$ and major $[Sc(NOTA)(OOCCH_3)]^{1-}$ peaks observed by ^{45}Sc NMR spectroscopy from $Na[Sc(NOTA)(OOCCH_3)]$ crystals dissolved in D_2O as a function of temperature. Peak deconvolution was performed using the "peak fitting" tool in MestreNova software V 14.1. The total peak area, $[Sc(NOTA)(OOCCH_3)]^{1-}$ + $[Sc(NOTA)(OOCCH_3)(H_2O)^{1-}]$, was normalized to 1.0 (100%), see ESI† for more details.

-0.0064 ± 0.0005 kcal mol^{-1} K^{-1}. As expected, these data suggested ΔS favored formation of reactants, $[Sc(NOTA)(OOCCH_3)]^{1-}$ and H_2O. This value was offset slightly by enthalpic stability that favored the $[Sc(NOTA)(OOCCH_3)(H_2O)]^{1-}$ product, which we attributed to formation of the Sc-H_2O bond. The entire process was close to thermoneutral at room temperature, with a calculated ΔG of $+0.2 \pm 0.2$ kcal mol^{-1} at T = 293.15 K. Overall, these values match the qualitative observation of more $[Sc(NOTA)(OOCCH_3)]^{1-}$ in solution compared to $[Sc(NOTA)(OOCCH_3)(H_2O)]^{1-}$ (roughly 1.5 : 1).

Calculated $[Sc(NOTA)(OOCCH_3)]^{1-}$ and $[Sc(NOTA)(OOCCH_3)(H_2O)]^{1-}$ coordination thermodynamics

To guide the interpretation of $[Sc(NOTA)(OOCCH_3)]^{1-}$ solution phase behavior, particularly in terms of interpreting the ^{45}Sc NMR results discussed above, density functional theory (DFT) calculations were performed. Emphasis was placed on assessing computationally determined *vs.* experimentally derived Gibbs free energy (ΔG) parameters associated with conversion of $Na[Sc(NOTA)(OOCCH_3)]$ and H_2O to $Na[Sc(NOTA)(OOCCH_3)(H_2O)]$. Note, these calculations included the $[Sc(NOTA)(OOCCH_3)]^{1-}$ and the Na^{1+} counter cation. Calculations were also made that accounted for potential coordination with DMSO. The calculated structure for $Na[Sc(NOTA)(OOCCH_3)]$ agreed well with the experimental data (Table 1 and in the ESI†). For instance, the calculations showed stable "in-cage" Sc^{3+} binding by $NOTA^{3-}$ with bidentate binding of $OOCCH_3{}^{1-}$. The calculated Sc–ligand distances were similar to those observed experimentally. One slight deviation was associated with the Sc–N_{NOTA} bond distances of the $NOTA^{3-}$ macrocyclic backbone. Here, theoretically predicted Sc–N_{NOTA} distances were slightly longer than the single crystal X-ray diffraction data by about +1.4% (on average). Similar differences in M–N distances between DFT optimized structures and X-ray diffraction data have been observed previously, specifically with $M(DOTP)^{5-}$ (M = Ac, Am, Cm, La)[57] and $M(HOPO)^{1-}$ (M = Am, Cm, Cf) complexes;[58] DOTP is 1,4,7,10-tetraazacyclododecane-1,4,7,10-tetra(methylene)phosphonic acid and HOPO is an octadentate hydroxypyridinone ligand. Usually, such discrepancies emerge when calculations focus on a single molecule and omit crystal packing effects from the extended solid, *e.g.* the presence of multiple counter cations surrounding each anion fragment (Fig. 2, see ESI†). It is also worth noting that the differences are relative to the static structure observed in the solid state, while the thermodynamic comparisons were made *versus* the solvated complex.

With a reasonable and validated calculated structure for $[Sc(NOTA)(OOCCH_3)]^{1-}$ in hand, two categories of reactions involving water with $Na[Sc(NOTA)(OOCCH_3)]$ were explored. We initially probed association of water to the complex to generate $Na[Sc(NOTA)(OOCCH_3)(H_2O)]$ (Fig. 4a and S15b†) and then interrogated acetate substitution by water to form $[Sc(NOTA)(H_2O)]$ or $[Sc(NOTA)(H_2O)_2]$ (Fig. 4b and S15b†). Acetate substitution by water was calculated to be highly unfavorable based on the large and positive ΔG values calculated for one (+18.17 kcal mol^{-1}) and for two (+24.94 kcal mol^{-1}) water molecules (see ESI†). In contrast, the calculations showed that water association was thermodynamically favorable with a small, slightly negative ΔG of -0.94 kcal mol^{-1}. A similar value of -0.74 kcal mol^{-1} was obtained if the calculations took into account a 1st-shell-hydrated Na^{1+} cation that stabilized $[Sc(NOTA)(OOCCH_3)]^{1-}$ complex, see ESI.† Both of these values were in exceptional agreement with the experimentally derived $+0.2 \pm 0.2$ kcal mol^{-1} at T = 293.15 K, especially when uncertainty between the

Table 1 Top: Selected bond distances (Å) and angles (°) from the Na[Sc(NOTA)(OOCCH$_3$)] crystal structure. Analogous bond distances or angles between the two [Sc(NOTA)(OOCCH$_3$)]$^{1-}$ fragments in the asymmetric unit are listed in the same row. Atomic numbering follows Fig. 1. Bottom: Comparative bond distances for Na[Sc(NOTA)(OOCCH$_3$)] from experimental X-ray crystallographic structure determination *vs.* DFT calculated structure

Experimental	Bond	Fragment 1 distance/angle (°/Å)	Bond	Fragment 2 distance/angle (°/Å)
Sc-NOTA	Sc1–N1	2.384(2)	Sc2–N4	2.376(2)
	Sc1–N2	2.374(2)	Sc2–N5	2.368(2)
	Sc1–N3	2.393(2)	Sc2–N6	2.436(2)
	Sc1–O1	2.116(1)	Sc2–O9	2.131(1)
	Sc1–O3	2.165(1)	Sc2–O11	2.158(1)
	Sc1–O5	2.155(1)	Sc2–O13	2.158(1)
Sc-OOCCH$_3$	Sc1–O7	2.377(1)	Sc2–O15	2.328(1)
	Sc1–O8	2.213(1)	Sc2–O16	2.180(1)
κ_2-(OOCCH$_3$)	O7–C13–O8	118.89(17)	O15–C27–O16	118.75(17)
	C13–O7	1.258(2)	C27–O15	1.262(2)
	C13–O8	1.283(2)	C27–O16	1.278(2)

		Average distance	
Theory	Bond	Experiment (avg., Å)	Theory (Å)
Sc-NOTA	Sc–O$_{NOTA}$	2.147 ± 0.019[a]	2.136
	Sc–N$_{NOTA}$	2.389 ± 0.025[a]	2.423
Sc-OOCCH$_3$	Sc–O$_{OOCCH_3}$ (short)	2.197 ± 0.023[a]	2.183
	Sc–O$_{OOCCH_3}$ (long)	2.353 ± 0.035[a]	2.357

[a] Error reported as the standard deviation of the mean at 1σ.

experimental and theoretically derived values were considered. These metrics suggested that this reaction was close to thermoneutral at room temperature. The computed ΔH (−4.58 kcal mol^{-1}) and ΔS (−0.01 kcal mol^{-1} K^{-1}) parameters were also in agreement with the values estimated from experiment (−1.7 ± 0.2 and −0.0064 ± 0.0005 kcal mol^{-1} K^{-1}, respectively), suggesting that the reaction was enthalpically favored. The small (close-to-zero) Gibbs free energy suggested that the [Sc(NOTA)(OOCCH$_3$)]$^{1-}$ and [Sc(NOTA)(OOCCH$_3$)(H$_2$O)]$^{1-}$ structures can coexist in solution. These computational results were consistent with the mixture of two species observed experimentally. In addition to the water addition/water-acetate substitution reactions, we also considered DMSO–acetate substitution and DMSO addition reactions with Na[Sc(NOTA)(OOCCH$_3$)]. Our calculations show that they are less thermodynamically favorable (Fig. S17 and S18†), with significantly more positive ΔG values in the range of +7.81–17.46 kcal mol^{-1} (eqn (S8)–(S10) in the ESI†) than the reaction of water association with Na[Sc(NOTA)(OOCCH$_3$)].

In the calculated water addition reaction, acetate slips from bidentate (κ^2-OOCCH$_3$$^{1-}$) to monodentate ($\kappa^1$-OOCCH$_3$$^{1-}$). This modification accommodated water occupation without increasing the Sc^{3+} coordination number beyond eight (Fig. 4, 6 and S12, S15a†). The calculated Sc–O$_{H_2O}$ (O9) distance was 2.374 Å and compared reasonably well with other analogous Sc–O$_{H_2O}$ experimental values.[42] It seemed likely that this calculated structure was further stabilized by hydrogen bonding between the coordinated H$_2$O ligand and the κ^1-OOCCH$_3$$^{1-}$ (Fig. 6).

It was important to evaluate the challenge associated with computationally determining the absolute value of Gibbs free energy for the hydration reactions considered. This exercise

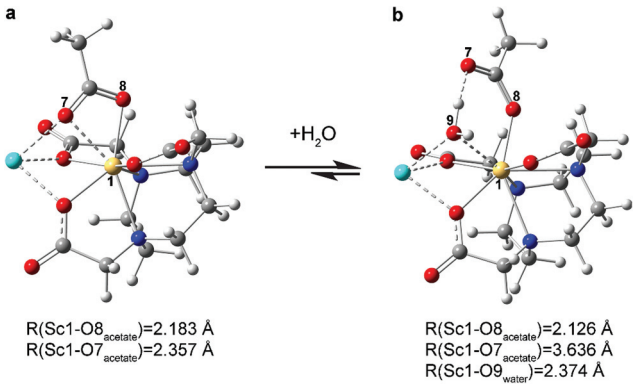

Fig. 6 Association of a water molecule to Na[Sc(NOTA)(OOCCH$_3$)]. Initially (a) the acetate is bound to Sc in a bidentate fashion (κ_2-OOCCH$_3$$^{1-}$); upon water coordination (b) the acetate slips to a monodentate binding mode (κ_1-OOCCH$_3$$^{1-}$).

put our calculated ΔG of −0.94 kcal mol^{-1} (−0.74 kcal mol^{-1} taking into account 1st-shell-hydrated Na^{1+} stabilizing [Sc(NOTA)(OOCCH$_3$)]$^{1-}$ complex) for the hydration reaction into perspective. To approximate hydrogen bonding interactions that occur in solution, we used clusters of water molecules based on previously determined global minima from the gas-phase calculations.[59] In this way, effects stemming from explicit waters of solvation were included, granted to a limited extent. The approach did not model dynamic hydrogen bonding interactions present in bulk water nor did it capture contributions from the outer sphere sodium cations. It did, however, provide a more reasonable alternative to ignoring bulk effects altogether (using a single water molecule on the

reactant side), which is well documented to severely overestimate ΔG.[57,58,60,61] It is worth noting that the calculated ΔG values fluctuated with sizes and shapes of water clusters considered in the hydration process for water association (see eqn (S4)–(7) in the ESI†). These results illustrate the challenge in determining the absolute values of ΔG for hydration reactions with high accuracy.

The DFT calculations provided guidance for interpreting what reactions were responsible for the exchange process observed experimentally (Fig. 3 and 4). These results attributed the two species observed by ^{45}Sc NMR spectroscopy to a mixture of $[Sc(NOTA)(OOCCH_3)]^{1-}$ and $[Sc(NOTA)(OOCCH_3)(H_2O)]^{1-}$. The calculated thermodynamic parameters were on the same order of magnitude (within a few kcal mol^{-1}) as the experimentally determined values. This interpretation was also self-consistent with the $H_2{}^{17}O$ labeled ^{45}Sc NMR experiment and the ^{45}Sc NMR experiment carried out in DMSO-d_6. Alternative mixtures, *e.g.* $[Sc(NOTA)(OOCCH_3)]^{1-}$ and $[Sc(NOTA)(H_2O)_n]$ (n = 1, 2), and $[Sc(NOTA)(OOCCH_3)]^{1-}$/$[Sc(NOTA)(DMSO)_n]$ (n = 1, 2), were discarded based on the massively positive calculated ΔG values.

Outlook

We have established an alternate synthetic approach that fully encapsulated Sc^{3+} into the $NOTA^{3-}$ binding pocket, providing the $Na[Sc(NOTA)(OOCCH_3)]$ complex in 69% isolated yield. Conditions for Sc^{3+} complexation by $NOTA^{3-}$ were identified that could be carried out under relatively mild conditions. The procedure successfully proceeded in aqueous media, under ambient atmosphere (air), in acetate buffer solutions [$HOOCCH_3$/$NaOOCCH_{3(aq)}$; 0.1 M] that were slightly acidic (pH = 5), and at relatively low temperatures (50 °C). Characterization in the solid-state showed that Sc^{3+} was bound "in-cage" by $NOTA^{3-}$. Achieving this "in-cage" binding required a gentle synthetic hand. For example, previous studies showed the ease at which "out-of-cage" binding prevailed. Only by heating Sc^{3+} with H_3NOTA, for longer reaction times, and in an acetic acid/acetate buffer solution did we generate an "in-cage" [Sc(NOTA)] complex.[36,38] Our [Sc(NOTA)] species was capped with a bidentate κ^2-$OOCCH_3{}^{1-}$ ligand, which provided stability (see below) and gave Sc^{3+} a coordination number of eight. Reaching steric saturation in aqueous media with only eight ligands also represented a distinction for Sc^{3+} in comparison to the larger lanthanide(III) cations, whose aqueous coordination numbers often range from 9–11.

Solution phase ^{45}Sc NMR studies demonstrated that the "in-cage" binding of Sc^{3+} by $NOTA^{3-}$ was preserved in aqueous solution. Computational results were consistent with this interpretation and suggested that in solution a mixture of $[Sc(NOTA)(OOCCH_3)]^{1-}$ and $[Sc(NOTA)(OOCCH_3)(H_2O)]^{1-}$ co-existed. These calculations were supported by ^{45}Sc NMR measurements made on $Na[Sc(NOTA)(OOCCH_3)]$ dissolved in water with $H_2{}^{17}O$. The presence of $H_2{}^{17}O$ dramatically enhanced relaxation of the ^{45}Sc resonance from $[Sc(NOTA)(OOCCH_3)(H_2{}^{17}O)]^{1-}$, as a result of the close ^{45}Sc–$^{17}O_{H2O}$ interaction. We interpret our results as suggesting that $[Sc(NOTA)(OOCCH_3)]^{1-}$ was the dominant species in solution and that the $[Sc(NOTA)(OOCCH_3)]^{1-}$ to $[Sc(NOTA)(OOCCH_3)(H_2O)]^{1-}$ ratio was ~1.5 to 1.

While characterizing the dynamic exchange behavior for conversion of $[Sc(NOTA)(OOCCH_3)]^{1-}$ to $[Sc(NOTA)(OOCCH_3)(H_2O)]^{1-}$, we identified the capping ligand(s) ($OOCCH_3{}^{1-}$ and H_2O) substantially influenced thermodynamic stability of $[Sc(NOTA)(L)_x]$ (L = capping ligands). Both $[Sc(NOTA)(OOCCH_3)]^{1-}$ and $[Sc(NOTA)(OOCCH_3)(H_2O)]^{1-}$ were calculated to be markedly more stable (by a ΔG of ~20 kcal mol^{-1}) than the simple hydrate, $[Sc(NOTA)(H_2O)_n]$ (n = 1 or 2). These results highlight the importance of the capping ligands (L) in a coordination complex with the general formula M(chelator)$(L)_x$; M being a metal like Sc^{3+} and chelator representing a binding agent like $NOTA^{3-}$. Our results suggest that the capping ligand is more than a simple ancillary ligand and can be used to influence M(chelator) stability.

Taken as a whole, the synthetic and computational assessment of "in-cage" Sc^{3+} binding by $NOTA^{3-}$ provided insight into rare-earth complexation chemistry, particularly for Sc^{3+}. The results highlighted how subtle variation for a given complexation method led to profoundly distinct outcomes, *e.g.* "in cage" and inert complexation *vs.* "out-of-cage" and labile binding. The data also piqued our interest in better defining the capping ligand's role in stabilizing rare-earth chelation complexes. Hence, current efforts are underway to further define Sc^{3+} speciation in aqueous media that contain a wider range of complexing agents and capping ligands. It is our aspiration that future studies carried out by us and others in the field will advance understanding of rare-earth complexation chemistry and contribute to developing the next generation of selective and strong binding rare-earth chelates. Success could impact rare-earth technologies broadly, and aid in solving 4f-element chelation changes.

Methods

General considerations

All reactions and manipulations were carried out in air at ambient pressures and temperatures. Anhydrous scandium(III) triflate [$Sc(OTf)_3$, Sigma-Aldrich, 99%], scandium(III) nitrate hexahydrate [$Sc(NO_3)_3{\cdot}6\ H_2O$, Sigma-Aldrich], 1,4,7-triazacyclononane-1,4,7-triacetic acid ($H_3NOTA{\cdot}3$ HCl, Macrocyclics), sodium acetate ($NaOOCCH_3$, Fischer), and sodium hydroxide (NaOH, pellets, Fischer) were used as received without further purification. Deuterated water (D_2O, Sigma-Aldrich) and deuterated dimethylsulfoxide (DMSO-d_6, 99.9%, anhydrous, Sigma-Aldrich), used as NMR spectroscopy solvents, were also purchased and used without further purification. Oxygen-17 enriched water ($H_2{}^{17}O$; estimated 90% ^{17}O) was procured from legacy chemical inventories at LANL, and had poorly identified origins. Isotopic enrichment was determined experimentally

prior to use. All pH measurements were made using Whatman pH paper (0–14 pH).

Instrumentation

NMR experiments were performed on a Bruker AVANCE™ 400 MHz solution spectrometer equipped with a 5 mm broadband tunable probe for X nuclei. Infrared spectra were collected on a commercial ThermoFisher Scientific Nicolet iS5 ATR-FTIR. High resolution mass spectrometry was performed on an Agilent 6210 LC-TOF (ESI, APCI, APPI).

Single crystal X-Ray diffraction

Data for Na[Sc(NOTA)(OOCCH$_3$)] were collected on a Bruker D8 Quest diffractometer configured with a CPAD Photon II™ area detector and MoKα (λ = 0.71073 Å) IμS 3.0 micro source™. The crystal was cooled to 100 K employing an Oxford Cryostream 800™ liquid nitrogen cryostat. A hemisphere of data was collected using omega scans and 1.00° frame widths. Data collection and initial indexing and cell refinement were handled using APEX 3 software.[62] Frame integration, including Lorentz-polarization corrections, and final cell parameter calculations were carried out using SAINT+ software.[63] The data were corrected for absorption using redundant reflections and the SADABS program.[64] The structure was solved using Intrinsic Phasing and difference Fourier techniques. All hydrogen atom positions were idealized, and rode on the atom to which they were attached. The final refinement included anisotropic temperature factors on all non-hydrogen atoms. Structure solution, refinement, graphics, and creation of publication materials were performed using SHELXTL.[54] Hydrogen atom positions were idealized, and all non-hydrogen atoms were refined anisotropically. Cell indexing, data collection, integration, structure solution, and refinement were performed using Bruker and SHELXTL software. Additional details are included in the ESI.†

CCDC deposit number: 2072300 and 2076191.†

Synthesis of sodium scandium(III) 1,4,7-triazacyclononane-1,4,7-triacetate κ_2-acetate, Na[Sc(NOTA)(OOCCH$_3$)]

A scintillation vial (20 mL) was loaded with Sc(OTf)$_3$ (49 mg, 0.1 mmol), a Teflon stir bar, and an aqueous solution of NaOOCCH$_3$ (8 mL; 0.1 M in NaOOCCH$_3$; pH = 5; adjusted by addition of acetic acid). Note, all pH measurements were determined using pH paper. Separately, H$_3$NOTA·3 HCl (41 mg, 0.1 mmol) was dissolved in an aqueous solution of NaOOCCH$_3$ (3 mL; 0.1 M NaOOCCH$_3$; pH = 4). This colorless aqueous solution of $H_{3-n}NOTA^{n-}$ was added dropwise to the stirring Sc solution described above. Upon addition the reaction solution pH dropped and was subsequently adjusted to a pH of 5 by dropwise addition of NaOH (2 M). Because the homogeneity of this solution is quite sensitive to the NaOH$_{(aq)}$ addition [*i.e.* rapid addition can result in $Sc(OH)_x^{n-}$ precipitate] the base was added slowly. The reaction solution was then heated to 50 °C and stirred overnight (~12 h). The solution was cooled and aqueous NaOH (2 M) was added to adjust the pH to 8. This caused unreacted Sc^{3+} to precipitate as scandium(III) hydroxide [$Sc(OH)_x(H_2O)_{9-x}^{3-x}$] and slight opacity of the initially transparent solution. The precipitate represented a small percentage of dissolved Sc^{3+} and was easily removed by passing the solution through a filter stick packed with filter paper and Celite. Collecting the transparent and colorless filtrate into a clean scintillation vial and removing the solvent by rotary evaporation yielded a white residue. The residue was extracted with a mixture of H$_2$O and MeOH (3 mL, 1 : 1, v : v). The extracts were filtered through Celite into a glass V-vial (10 mL) and the filtrate was carefully layered with acetone (1 mL). This solution was then stored at 10 °C for 1 week. From the crystallization solution, colorless plate-like crystals formed (18 mg, 41% yield) that were suitable for characterization by single crystal X-ray diffraction. Addition of more acetone (1.5 mL) to the equilibrated solution produced a second crop of crystals (12 mg, 28%). After drying the crystals, the total crystalline yield for Na[Sc(NOTA)(OOCCH$_3$)] was 69%.

NMR: ^{1}H (D$_2$O, 20 °C, 400.13 MHz): δ 3.69 (br, s), 3.54 (br, s), 2.95 (br, m), 1.78 (s, OOCC*H*$_3$). ^{1}H (DMSO-d_6, 20 °C, 400.13 MHz): δ 3.50 (br, s), 3.39 (s), 3.12 (br, m), 2.91 (br, m), 1.83 (s). ^{45}Sc (D$_2$O, 20 °C, 97.198 MHz): δ 99.8 ppm (fitted peak width, 840 Hz), 88.8 ppm (fitted peak width, 440 Hz). ^{45}Sc (DMSO-d_6, 20 °C, 97.198 MHz): δ 99.47 ppm (fitted peak width, 3744 Hz).

IR (cm^{-1}): 3370 (br, m); 3130 (s); 3040 (s), 2860 (br, shoulder); 1630 (br, shoulder), 1570 (s); 1400 (s). See ESI† for spectra and additional details.

HRMS [Sc(NOTA)]: (ToF, positive ion mode) $ScN_3O_6C_{12}H_{19}$ $(M + H)^+$ 346.0827, observed 346.0841; $ScNaN_3O_6C_{12}H_{18}$ $(M + Na)^+$ 368.0658, observed 368.0647.

Computational details

All complexes were optimized without any constraints using self-consistent reaction field approach based on the integral equation formalism of the polarized continuum model (PCM)[65,66] as implemented in Gaussian 16 software package (Version B.01).[67] Water and dimethylsulfoxide (DMSO) were used as solvents in the respective reactions. Harmonic frequency calculations were performed to confirm that the optimized structures were stationary points on the potential energy surface. The initial geometry of the Na[Sc(NOTA)(OOCCH$_3$)] complex was taken from the experimental XRD data. Energies and geometries were reported from results using the PBE0[68] hybrid DFT functional and def2-TZVP[69] triple zeta valence basis set. Dispersion corrections (D3)[70] were applied to account for possible intramolecular noncovalent interactions that can be important for the correct description of solvent-complex interaction. As reported previously for various transition-metal-based complexes,[71] PBE0-D3 was found to be the best functional in the complete benchmark set relative to estimated CCSD(T)/CBS reference data, with a mean absolute deviation from the reference values of 1.1 kcal mol^{-1}. Wavefunctions of the studied species were found to be stable, indicating that the calculations converged to the ground electronic state. Water clusters containing 16–19 molecules were used to more accurately calculate the energy of water binding/

exchange between bulk water and complexes. Using only a single water molecule would neglect the energy from hydrogen bonding in water clusters and lead to less accurate ΔG values. The geometries of these water clusters were taken from the previously established global minima gas-phase structures,[59] and were fully optimized in solvent medium using the PCM model in this study.

Conflicts of interest

The authors declare no competing financial interests.

Acknowledgements

We acknowledge the US Department of Energy, Office of Science, Office of Basic Energy Sciences, Heavy Element Chemistry program (2020LANLE372) and LANL's LDRD-DR project (20180005DR) for support. Los Alamos National Laboratory is operated by Triad National Security, LLC, for the National Nuclear Security Administration of US Department of Energy (contract no. 89233218CNA000001). We are grateful for postdoctoral support provided (in-part) by the Glenn T. Seaborg Institute (KEA), by the LANL Director's Fellowship Program (SMG), and by the J. Robert Oppenheimer Distinguished Postdoctoral Fellowship (IAP). I. A. P. acknowledges the computational resources at the ARCC HPC cluster at the University of Akron. We would like to thank Mr Saman Shafaie and the Northwestern University IMSERC for performing the HRMS analyses.

Notes and references

1 Z. Guo and P. J. Sadler, *Adv. Inorg. Chem.*, 2000, **49**, 183–306.
2 N. Farrell, *Coord. Chem. Rev.*, 2002, **232**, 1–4.
3 K. D. Mjos and C. Orvig, *Chem. Rev.*, 2014, **114**, 4540–4563.
4 J. Karges, *ChemBioChem*, 2020, **21**, 3044–3046.
5 B. A. Corbin, A. C. Pollard, M. J. Allen and M. D. Pagel, *Mol. Imaging Biol.*, 2019, **21**, 193–199.
6 K. J. Franz and N. Metzler-Nolte, *Chem. Rev.*, 2019, **119**, 727–729.
7 A. J. Dos santos-García, M. Á. Alario-Franco and R. Sáez-Puche, Lanthanides: Superconducting Materials, in *Encyclopedia of Inorganic and Bioinorganic Chemistry*, ed. R. A. Scott, 2012, DOI: 10.1002/9781119951438.eibc2039.
8 J. E. McPeak, S. S. Eaton and G. R. Eaton, *Electron paramagnetic resonance of lanthanides*, Elsevier Inc., 1st edn, 2021, vol. 651.
9 D. Parker, E. A. Suturina, I. Kuprov and N. F. Chilton, *Acc. Chem. Res.*, 2020, **53**, 1520–1534.
10 J. C. G. Bünzli, *Handb. Phys. Chem. Rare Earths*, 2016, **50**, 141–176.
11 D. Parker, J. D. Fradgley and K. L. Wong, *Chem. Soc. Rev.*, 2021, **50**, 8193–8213.
12 S. V. Eliseeva and J. C. G. Bünzli, *Chem. Soc. Rev.*, 2010, **39**, 189–227.
13 C. Müller, K. A. Domnanich, C. A. Umbricht and N. P. Van Der Meulen, *Br. J. Radiol.*, 2018, **91**, 1–13.
14 R. F. Cavaier, F. Haddad, T. Sounalet, T. Stora and I. Zahi, *Phys. Procedia*, 2017, **90**, 157–163.
15 F. D. C. Guerra Liberal, A. A. S. Tavares and J. M. R. S. Tavares, *Appl. Radiat. Isot.*, 2016, **110**, 87–99.
16 S. J. Goldsmith, *Semin. Nucl. Med.*, 2020, **50**, 87–97.
17 C. Müller, K. Zhernosekov, U. Köster, K. Johnston, H. Dorrer, A. Hohn, N. T. Van Der Walt, A. Türler and R. Schibli, *J. Nucl. Med.*, 2012, **53**, 1951–1959.
18 R. P. Baum, A. Singh, M. Benešová, C. Vermeulen, S. Gnesin, U. Köster, K. Johnston, D. Müller, S. Senftleben, H. R. Kulkarni, A. Türler, R. Schibli, J. O. Prior, N. P. Van Der Meulen and C. Müller, *Dalton Trans.*, 2017, **46**, 14638–14646.
19 C. Müller, C. A. Umbricht, N. Gracheva, V. J. Tschan, G. Pellegrini, P. Bernhardt, J. R. Zeevaart, U. Köster, R. Schibli and N. P. van der Meulen, *Eur. J. Nucl. Med. Mol. Imaging*, 2019, **46**, 1919–1930.
20 A. K. M. Rahman and A. Awal, *J. Radioanal. Nucl. Chem.*, 2020, **323**, 731–740.
21 C. Vermeulen, G. F. Steyn, F. Szelecsényi, Z. Kovács, K. Suzuki, K. Nagatsu, T. Fukumura, A. Hohn and T. N. Van Der Walt, *Nucl. Instrum. Methods Phys. Res., Sect. B*, 2012, **275**, 24–32.
22 E. Hindie, P. Zanotti-Fregonara, M. A. Quinto, C. Morgat and C. Champion, *J. Nucl. Med.*, 2016, **57**, 759–764.
23 C. Champion, M. A. Quinto, C. Morgat, P. Zanotti-Fregonara and E. Hindié, *Theranostics*, 2016, **6**, 1611–1618.
24 C. Müller, E. Fischer, M. Behe, U. Köster, H. Dorrer, J. Reber, S. Haller, S. Cohrs, A. Blanc, J. Grünberg, M. Bunka, K. Zhernosekov, N. van der Meulen, K. Johnston, A. Türler and R. Schibli, *Nucl. Med. Biol.*, 2014, **41**, e58–e65.
25 C. Müller, M. Bunka, J. Reber, C. Fischer, K. Zhernosekov, A. Türler and R. Schibli, *J. Nucl. Med.*, 2013, **54**, 2168–2174.
26 P. Santhanam, D. Taieb, L. Solnes, W. Marashdeh and P. W. Ladenson, *Clin. Endocrinol.*, 2017, **86**, 645–651.
27 S. Ferguson, H. S. Jans, M. Wuest, T. Riauka and F. Wuest, *EJNMMI Phys.*, 2019, **6**, 1–14.
28 G. A. Wiseman, K. Pacak, M. S. O'Dorisio, D. R. Neumann, A. D. Waxman, D. A. Mankoff, S. I. Heiba, A. N. Serafini, S. S. Tumeh, N. Khutoryansky and A. F. Jacobson, *J. Nucl. Med.*, 2009, **50**, 1448–1454.
29 E. Eppard, A. de la Fuente, M. Benešová, A. Khawar, R. A. Bundschuh, F. C. Gärtner, B. Kreppel, K. Kopka, M. Essler and F. Rösch, *Theranostics*, 2017, **7**, 4359–4369.
30 S. M. Qaim, B. Scholten and B. Neumaier, *J. Radioanal. Nucl. Chem.*, 2018, **318**, 1493–1509.
31 J. H. Turner, *Br. J. Radiol.*, 2018, **91**, 1–9.
32 C. S. Loveless, L. L. Radford, S. J. Ferran, S. L. Queern, M. R. Shepherd and S. E. Lapi, *EJNMMI Res.*, 2019, **9**, 1–10.
33 B. A. Vaughn, A. J. Koller and E. Boros, in *Methods in Enzymology*, Elsevier Inc., 1st edn, 2021, vol. 651, pp. 343–371.

34 B. A. Vaughn, S. H. Ahn, E. Aluicio-Sarduy, J. Devaraj, A. P. Olson, J. Engle and E. Boros, *Chem. Sci.*, 2020, **11**, 333–342.
35 M. Połosak, A. Piotrowska, S. Krajewski and A. Bilewicz, *J. Radioanal. Nucl. Chem.*, 2013, **295**, 1867–1872.
36 S. Huclier-Markai, A. Sabatie, S. Ribet, V. Kubíček, M. Paris, C. Vidaud, P. Hermann and C. S. Cutler, *Radiochim. Acta*, 2011, **99**, 653–662.
37 A. Majkowska-Pilip and A. Bilewicz, *J. Inorg. Biochem.*, 2011, **105**, 313–320.
38 M. Pniok, V. Kubíček, J. Havlíčková, J. Kotek, A. Sabatie-Gogová, J. Plutnar, S. Huclier-Markai and P. Hermann, *Chem. – Eur. J.*, 2014, **20**, 7944–7955.
39 M. L. Williams, *Occup. Environ. Med.*, 1996, **53**, 504.
40 S. Huclier-Markai, R. Kerdjoudj, C. Alliot, A. C. Bonraisin, N. Michel, F. Haddad and J. Barbet, *Nucl. Med. Biol.*, 2014, **41**, e36–e43.
41 R. Kerdjoudj, M. Pniok, C. Alliot, V. Kubíček, J. Havlíčková, F. Rösch, P. Hermann and S. Huclier-Markai, *Dalton Trans.*, 2016, **45**, 1398–1409.
42 G. Nagy, D. Szikra, G. Trencsényi, A. Fekete, I. Garai, A. M. Giani, R. Negri, N. Masciocchi, A. Maiocchi, F. Uggeri, I. Tóth, S. Aime, G. B. Giovenzana and Z. Baranyai, *Angew. Chem., Int. Ed.*, 2017, **56**, 2118–2122.
43 J. Sinnes, J. Nagel and F. Rösch, *EJNMMI Radiopharm. Chem.*, 2019, **4**, 1–10.
44 B. A. Vaughn, A. J. Koller, Z. Chen, S. H. Ahn, C. S. Loveless, S. J. Cingoranelli, Y. Yang, A. Cirri, C. J. Johnson, S. E. Lapi, K. W. Chapman and E. Boros, *Bioconjugate Chem.*, 2021, **32**, 1232–1241.
45 S. Aime, A. Barge, F. Benetollo, G. Bombieri, M. Botta and F. Uggeri, *Inorg. Chem.*, 1997, **36**, 4287–4289.
46 F. Benetollo, G. Bombieri, L. Calabi, S. Aime and M. Botta, *Inorg. Chem.*, 2003, **42**, 148–157.
47 P. Vojtíšek, P. Cígler, J. Kotek, J. Rudovský, P. Hermann and I. Lukeš, *Inorg. Chem.*, 2005, **44**, 5591–5599.
48 F. Benetollo, G. Bombieri, L. Calabi, S. Aime and M. Botta, *Inorg. Chem.*, 2003, **42**, 148–157.
49 C. Kumas, W. S. Fernando, P. Zhao, M. Regueiro-Figueroa, G. E. Kiefer, A. F. Martins, C. Platas-Iglesias and A. D. Sherry, *Inorg. Chem.*, 2016, **55**, 9297–9305.
50 K. J. Miller, A. A. Saherwala, B. C. Webber, Y. Wu, A. D. Sherry and M. Woods, *Inorg. Chem.*, 2010, **49**, 8662–8664.
51 J. Blahut, P. Hermann, Z. Tošner and C. Platas-Iglesias, *Phys. Chem. Chem. Phys.*, 2017, **19**, 26662–26671.
52 A. L. Spek, *Acta Crystallogr., Sect. C: Struct. Chem.*, 2015, **71**, 9–18.
53 O. V. Dolomanov, L. J. Bourhis, R. J. Gildea, J. A. K. Howard and H. Puschmann, *J. Appl. Crystallogr.*, 2009, **42**, 339–341.
54 G. M. Sheldrick, *SHELXTL*, University of Gottingen, Germany, 2016.
55 J. Mason, *Multinuclear NMR*, Plenum Press, New York, 6th edn, 1987.
56 A. Abragam, *The Principles of Nuclear Magnetism*, Clarendon Press, 1961.
57 B. W. Stein, A. Morgenstern, E. R. Batista, E. R. Birnbaum, S. E. Bone, S. K. Cary, M. G. Ferrier, K. D. John, J. L. Pacheco, S. A. Kozimor, V. Mocko, B. L. Scott and P. Yang, *J. Am. Chem. Soc.*, 2019, **141**, 19404–19414.
58 M. P. Kelley, G. J. P. Deblonde, J. Su, C. H. Booth, R. J. Abergel, E. R. Batista and P. Yang, *Inorg. Chem.*, 2018, **57**, 5352–5363.
59 J. T. Su, X. Xu and W. A. Goddard III, *J. Phys. Chem. A*, 2004, **108**(47), 10518–10526.
60 M. P. Kelley, J. Su, M. Urban, M. Luckey, E. R. Batista, P. Yang and J. C. Shafer, *J. Am. Chem. Soc.*, 2017, **139**, 9901–9908.
61 X. Cao, D. Heidelberg, J. Ciupka and M. Dolg, *Inorg. Chem.*, 2010, **49**, 10307–10315.
62 *APEX3*, Bruker, AXS Inc., Madison, Wisconsin, 2019.
63 *SAINT+*, Bruker, AXS Inc., Madison, Wisconsin, 2013.
64 L. Krause, R. Herbst-Irmer, G. M. Sheldrick and D. Stalke, *J. Appl. Crystallogr.*, 2015, **48**, 3–10.
65 B. Mennucci, E. Cancès and J. Tomasi, *J. Phys. Chem. B*, 1997, **101**, 10506–10517.
66 E. Cancès and B. Mennucci, *J. Math. Chem.*, 1998, **23**, 309–326.
67 M. J. Frisch, G. W. Trucks, H. B. Schlegel, G. E. Scuseria, M. A. Robb, J. R. Cheeseman, G. Scalmani, V. Barone, G. A. Petersson, H. Nakatsuji, X. Li, M. Caricato, A. V. Marenich, J. Bloino, B. G. Janesko, R. Gomperts, B. Mennucci, H. P. Hratchian, J. V. Ortiz, A. F. Izmaylov, J. L. Sonnenberg, D. Williams-Young, F. Ding, F. Lipparini, F. Egidi, J. Goings, B. Peng, A. Petrone, T. Henderson, D. Ranasinghe, V. G. Zakrzewski, J. Gao, N. Rega, G. Zheng, W. Liang, M. Hada, M. Ehara, K. Toyota, R. Fukuda, J. Hasegawa, M. Ishida, T. Nakajima, Y. Honda, O. Kitao, H. Nakai, T. Vreven, K. Throssell, J. A. Montgomery Jr., J. E. Peralta, F. Ogliaro, M. J. Bearpark, J. J. Heyd, E. N. Brothers, K. N. Kudin, V. N. Staroverov, T. A. Keith, R. Kobayashi, J. Normand, K. Raghavachari, A. P. Rendell, J. C. Burant, S. S. Iyengar, J. Tomasi, M. Cossi, J. M. Millam, M. Klene, C. Adamo, R. Cammi, J. W. Ochterski, R. L. Martin, K. Morokuma, O. Farkas, J. B. Foresman and D. J. Fox, Gaussian, Inc., Wallingford CT, 2016.
68 C. Adamo and V. Barone, *J. Chem. Phys.*, 1999, **110**, 6158–6170.
69 F. Weigend and R. Ahlrichs, *Phys. Chem. Chem. Phys.*, 2005, **7**, 3297–3305.
70 S. Grimme, J. Antony, S. Ehrlich and H. Krieg, *J. Chem. Phys.*, 2010, **132**, 132.
71 M. Steinmetz and S. Grimme, *ChemistryOpen*, 2013, **2**, 115–124.